Single Electron Traps at the Surface of Polycrystalline MgO: Assignment of the Main Trapping Sites

Mario Chiesa, Maria Cristina Paganini, Giuseppe Spoto, and Elio Giamello*

Dipartimento di Chimica IFM, Università di Torino, via P. Giuria 7, 10125 Torino, Italy

Cristiana Di Valentin, Annalisa Del Vitto, and Gianfranco Pacchioni

Dipartimento di Scienza dei Materiali, Università di Milano-Bicocca, via R. Cozzi 53, 20125 Milano, Italy

Received: November 15, 2004; In Final Form: January 25, 2005

Paramagnetic centers at the surface of ionic oxides in the form of trapped electrons can be generated by exposure of the material to alkali metal or hydrogen atoms or of molecular hydrogen under UV irradiation. For many years, it has been assumed that the resulting paramagnetic centers consist of oxygen vacancies filled by one electron. High-resolution electron spin resonance spectra and ab initio quantum chemical calculations show that the paramagnetic centers consist of $(H^+)(e^-)$ electron pairs formed at morphological irregularities of the surface. At least three different kinds of $(H^+)(e^-)$ centers, [A], [B], and [C], have been identified with abundances of 80%, 10%, and 8%, respectively. In this work, we compare a wide set of measured and computed g-factors and hyperfine coupling constants of the unpaired electron with the surrounding ^{25}Mg, ^{17}O, and ^{1}H nuclei and we propose a general assignment of the centers. $(H^+)(e^-)$ pairs formed at Mg_{4c} ions at steps and edges account for species [A], centers formed at Mg_{4c} ions at reverse corners correspond to species [B], and species [C] originates from $(H^+)(e^-)$ pairs formed at Mg_{3c} ions at corners and kinks.

1. Introduction

The phenomenon of electron trapping into the bulk or at the surface of solid materials is attracting the attention of numerous research groups in chemistry. Electron trapping is related, for instance, to the area of electrides, materials able to trap stoichiometric amounts of electrons in the bulk of a solid[1,2] or in the cavities of microporous systems such as zeolites.[3,4] Electron trapping is also crucial in phenomena like the charge separation that occurs spontaneously or by photoionization when particular molecules are introduced in the channels of microporous aluminosilicates.[5,6] In the latter case, a carbocation and an electron are formed and the stabilization of the latter one is the crucial, not fully understood, step of the whole phenomenon which can be of relevance in the field of energy storage.

The activity of our research groups has been focused in the past on the investigation of electron trapping at the surface of polycrystalline insulating oxides (and in particular of alkali earth oxides such as MgO and CaO) with two principal scopes. The first one was the use of trapped electrons or trapped holes as probes to describe in detail the surroundings of the trapped site. Our strategic goal has been that of describing the surface features of a finely divided oxide at a level comparable to that attained by modern surface science for single crystal faces or thin films. The second scope was the study of ionization and charge separation phenomena at the surface and of the reactivity of surface stabilized carriers in electron transfer and other elementary reactions. The natural technique to exploit the capacity of surface trapped carriers as structural probes is electron paramagnetic resonance (EPR), a technique extremely efficient in describing paramagnetic centers and widely used also in the characterization of defects in the bulk and at the surface of solid materials.

Among the surface defects of oxides, ion vacancies are particularly important, and a remarkable effort has been produced in the last 10 years aimed at their identification and characterization on both polycrystalline[7−9] and thin films systems.[7,8] As a bare ion vacancy, i.e., a vacancy with no trapped electrons, usually referred to as the F_S^{2+} center, is not easily detected by spectroscopic techniques (only very recently direct observations of oxygen vacancies on metal oxides became possible through STM),[9,10] the activity aimed to unravel the nature and location of such defects has been based on indirect methods. Because of the natural propensity of an anion vacancy for electron trapping, the use of electrons as vacancy probes was identified as a possible method to reveal such defects at the surface of ionic oxides such as MgO and CaO.[11−14]

Doping of the ionic oxide surface with excess electrons is achieved in two main ways: adsorption of atoms (alkali metals, atomic hydrogen) or UV irradiation of the solid in the presence of molecular hydrogen.[15,16] Incidentally, the dissociative adsorption of H_2 on MgO (which is the subject of a great deal of activity in surface chemistry)[17] is the first step of the formation of a trapped electron center upon UV light irradiation. Both methods described above actually have a common point represented by the ionization of atoms at a particular location of the surface with consequent formation of a trapped electron and a positive ion

$$H^{\bullet} + Mg_n^{2+}\,O^{2-} \rightarrow \begin{matrix} e^- & H \\ Mg_n^{2+} & O^- \end{matrix} \qquad (1)$$

In the above reaction the symbol Mg_n^{2+} ($n \geq 1$) represents an electron trap i.e., in principle, a single ion or an array of ions capable of stabilizing an unpaired electron.

* To whom correspondence should be addressed. Tel: ++39-011-6707574. Fax: ++39-011-6707855. E-mail: elio.giamello@unito.it.

10.1021/jp044783c CCC: $30.25
Published on Web 03/19/2005

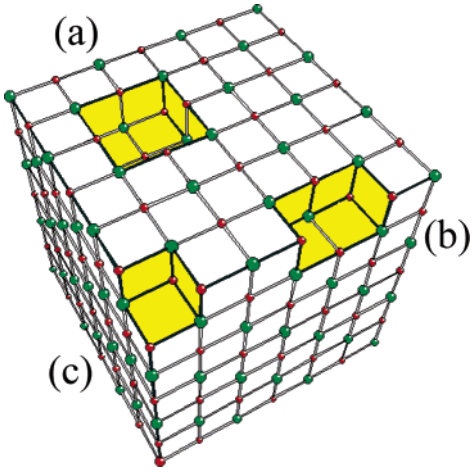

Figure 1. Schematic representation of oxygen vacancies at the surface of a cubic ionic oxide. (a) terrace; (b) edge; (c) corner.

The concept of a surface electron trapping center in ionic oxides has undergone substantial evolution in the past 30 years. The early models, due to the seminal work of Tench,[18] imply that trapped electrons are localized in 5-fold coordinated oxygen vacancies located on the (100) face of the surface (Figure 1a). Such crystal face is by far the dominant one in polycrystalline MgO and CaO. The Tench model was the natural extension to the surface of the classic de Boer's model for bulk F centers (electrons trapped in 6-fold coordinated vacancies).[19] This model (initially supported by the fact that also surface trapped electrons cause the coloring of the transparent ionic oxide which turns to blue after the described treatment) became progressively outdated on the basis of successive activity. In the last 5 years, in fact, several alternative models have been proposed for trapping centers, ranging from low-coordinated vacancies at steps and corners (Figure 1b, 1c) to neutral divacancies[20,21] or morphological defects such as the reverse corner[16] (RC). This latter site, with the trap built up by three Mg^{2+}ions, is interesting for two reasons: first, it is capable of heterolythic dissociation of molecular hydrogen (1) and, second, it belongs to a class of morphological features of the surface which are neutral and thus conceptually different from the charged oxygen vacancies, F_S^{2+}, proposed in the past. The most critical point of the Tench model was in fact connected to the high energetic cost for the formation of a bare anion vacancy (Fs^{2+}), which must correspond to a low abundance of such defect in a solid in thermodynamic equilibrium. With the RC site, a novel class of surface sites was therefore introduced in the debate on the surface traps of ionic oxides.

More recently a further achievement in this field consisted in understanding that also single, three-coordinated, Mg^{2+} cations located at kinks or corners of the crystals can act as surface electron traps. These low coordinated ions are actually expected to be "shallow traps" in the band gap,[22] and for this reason, the electrons occupying these levels are easily ionized and cannot constitute true "color centers". However, when the surface is populated according to reaction 1 the proton, H^+, bound to an oxide anion near the trapped electron exerts a stabilizing action on this latter one lowering the energy of the corresponding state and transforming the center in a true, thermally stable, surface color center.[23] Experimental−theoretical evidence of a center based on an electron trapped at a single three-coordinated Mg^{2+} cation and stabilized by a nearby OH group was recently given by some of us.[23]

On the basis of what resumed above, it should be clear that the ideas on surface electron trapping on insulating oxides are progressively evolving. The present article aims to propose a thorough and possibly conclusive assignment of the whole trapped electron centers present on fully dehydrated MgO. This is now possible as the main limitation encountered in the past when studying EPR spectra of surface trapped electrons, i.e., the small differences between the overlapped EPR signals corresponding to different centers, has been overcome using particular procedures for creating the centers and coloring the solid. These are (i) the rapid quenching of the activated solid at the end of thermal activation and (ii) the use of more powerful sources to color the system kept under hydrogen. Using this experimental approach, high-intensity EPR spectra with new distinct resolved hyperfine structures due to $^{25}Mg^{2+}$ ions (not clearly detected in previous experiments) are observed in addition to the already known data. Furthermore, it has been possible to prepare ^{17}O enriched MgO samples thus opening the possibility to detect at the same time the hyperfine coupling with the cations and anions surrounding the trapped electron. The whole set of data is used here for comparison with theoretical calculations to propose structural assignments based on new and more realistic grounds. Theoretical modeling is essential in our approach to bridge the experimental datum with a realistic structural model. In particular, by calculating the electron spin density on all of the nuclei surrounding the trapped electron, it is possible to discriminate among models of the various sites present at the surface and to identify those corresponding to the sites actually observed in the experiment. Furthermore, besides the hyperfine interactions of the unpaired electron with the surrounding nuclei, the electronic g-factors for the surface paramagnetic centers are computed here for the first time and compared with the experimental ones. The continuous feed-back between experiments and theory has been thus the decisive factor to achieve the assignments reported in this work.

2. Experimental Details

The experiments were carried out with two types of polycrystalline MgO. The first one was obtained by chemical vapor deposition (CVD) in a flow system[24] and kindly supplied by Prof. Erich Knözinger (Institut für Physikalische Chemie Technische Universität Wien). The second one was produced by thermal decomposition of $Mg(OH)_2$ under dynamic vacuum at 523 K for 16 h.

A fraction of all samples were activated by the previously described procedure[25] consisting in a thermal treatment at 1173 K under dynamic vacuum in order to obtain a totally dehydroxylated surface. This is followed by slow cooling to room temperature. The resulting surface area (measured by the B.E.T. method) after this treatment was $\approx$320 $m^2\ g^{-1}$ for the CVD sample and $\approx$200 $m^2\ g^{-1}$ for the ex-hydroxide.

For a second fraction of the samples, a different procedure was adopted building up and using for activation a special cell which allows a very rapid transfer of the sample from the region at 1173 K to the EPR tube kept in liquid nitrogen (77 K). By this rapid quenching procedure (as it will be shown in the following), a higher fraction of defective and low coordination sites remains at the surface of the oxide in comparison with the unquenched sample.

A thorough description of the methodology used in the preparation of the surface color centers has been reported elsewhere.[25] A brief summary is given here. Hydrogen or deuterium ($\sim$100 Torr, 1 Torr = 133 Pa) was added to the activated oxide at 298 K, and the powder was subsequently cooled to 77 K. The sample was then irradiated using a 500 W Oriel Instruments UV lamp, incorporating a Hg/Xe arc lamp

(250 nm to > 2500 nm) in conjunction with a water filter. The UV output below 280 nm accounts for only 4 to 5% of the total lamp output.

The EPR spectra were recorded at 298 K on a Bruker EMX spectrometer operating at X-band frequencies and on a Bruker 300 machine operating in the Q-band mode.

Transmission electron micrographs were obtained with a JEOL JEM 2000EX HRTEM microscope equipped with a top-entry stage and operating at 200 kV. The MgO sample (previously treated at 1073 K) was in powdered form dispersed on a holey-carbon grid.

3. Computational Details

The spin properties of single trapped electrons at low-coordinated sites of the MgO surface have been computed by electronic structure calculations of the trap center with the help of quantum chemical embedded cluster models. In particular g-factor shifts due to existing local fields as a consequence of an anisotropic environment, and hyperfine interaction of the electron spin with the nuclear spin of the ^{17}O, ^{25}Mg, and ^{1}H nuclides have been determined. The calculations have been performed at the density functional theory (DFT) level, using the gradient corrected Becke's three parameters hybrid exchange functional,[26] in combination with the correlation functional of Lee, Yang, and Parr[27] (B3LYP).

The effective g-factor is given in terms of the 3×3 g-matrix that describes the coupling between the spin system and the external magnetic field according to the Hamiltonian: $\mathbf{H}_{spin} = \beta\mathbf{BgS}$. The observable parts of the g-matrix are the square roots of the eigenvalues of $\mathbf{g}^T\mathbf{g}$, which can be predicted from density functional theory.[28,29] The hyperfine spin-Hamiltonian, $\mathbf{H}_{hfc} = \mathbf{SAI}$, is given in terms of the hyperfine matrix A which describes the coupling of the electron with the nuclear spin.[28] The components of A can be represented as the sum of an isotropic part, a_{iso}, related to the Fermi contact term, and the matrix B which represents the classical dipolar interaction between two magnetic (electron and nuclear) moments. Typical anisotropic interactions can be observed when the unpaired electron is in directional orbitals such as p, d, f, etc. The matrix notation for A tensor is: $A = a_{iso}\, U + B$.

Due to the highly ionic nature of MgO, the truncation of the crystal lattice implies the use of an external field to represent the long-range Coulomb potential. The quantum-mechanically treated cluster is thus embedded in an array of about 900 classical polarizable ions (shell model) surrounded by a matrix of about 3000 ± 2 classical nonpolarizable ions (point charges).[30] The interface between QM cluster and classical ions includes Mg ions which are represented by semi-local effective core potential[31] (ECP) to prevent an artificial polarization of the oxygen anions of the QM cluster. The interactions between QM atoms and classical atoms and those among classical ions are described with the use of classical potentials. All QM atoms and classical polarizable ions are allowed to relax simultaneously during the geometry optimization. Through this approach it is possible to describe both long-range polarization and relaxation effects. It is implemented in the GUESS code,[30] which provides the shell model representation for the classically treated part of the system and an interface with the Gaussian 98[32] package for ab initio calculations of the QM cluster.

Five kinds of electron traps have been analyzed. Three of them correspond to a $(H^+)(e^-)$ pair formed on an $O_{4c}-Mg_{4c}$ pair at the morphological defects sites of step, edge and reverse corner. The remaining other two correspond to a $(H^+)(e^-)$ pair formed on an $O_{4c}-Mg_{3c}$ pair at the morphological defects sites of corner and kink. The cluster used, $[Mg_{12}O_{13}(H)]_{step}$, $[Mg_{12}O_{12}(H)]_{edge}$, $[Mg_{17}O_{17}(H)]_{reverse\ corner}$, $[Mg_{13}O_{13}(H)]_{kink}$, and $[Mg_4O_4(H)]_{corner}$, are globally neutral. Moreover a $(H^+)(e^-)$ pair formed on a terrace oxygen vacancy $F_s(H)^+$, $[Mg_{17}O_{17}(H)]_{terrace}{}^+$, is reported for comparison.

Different basis-set extensions have been applied for geometry optimization and for EPR properties computation. A 6-31G basis set on all Mg and O ions and 6-311+G** on H,[33,34] has been used for geometry optimization, whereas the g-tensor and the hyperfine coupling constants (hfcc) have been obtained performing single point calculation on the optimized geometry using a more flexible basis set, with 6-311+G* on Mg and EPR−II on O and on H. The EPR−II basis set has been specifically designed to accurately reproduce the hfcc of O-containing radicals.[35] The choice of the exchange functional affects, to some extent, the computed EPR properties. This aspect has been discussed in detail, for the computation of the hfcc, by Barone,[35] who has shown that in general, and in particular for ^{17}O, the B3LYP functional used here gives the best agreement with the experiment. For the computation of g-factors, Neese[29] has presented some interesting results on small radicals obtained on the basis of Hartree−Fock and Kohn−Sham theories. Comparison with experimental data shows that it is difficult to measure g shifts more accurately than about 10^{-3}. Thus, according to Neese,[29] a deviation of 500 ppm between theory and experiment falls within the error bars of the experiment and even an agreement within 1000 ppm is considered as satisfactory.

To test the ability of our methods to describe hyperfine coupling constants of these type of neutral trapping centers, we have computed the same quantities for magnesium hydroxide (MgOH) and magnesium hydride (MgH) molecular radicals, for which experimental data in the Ne matrix is available for direct comparison.[36] In the MgOH radical, the unpaired electron is highly localized on the Mg^+ ion. Interaction of the unpaired electron with the ^{25}Mg and the ^{1}H nuclei has been measured. We localized two conformational minima on the potential energy surface. One is the linear MgOH radical, the other, slightly more stable (0.05 eV), is the bent structure with a Mg−O−H angle of 133. Only the former, with axial symmetry, has been characterized experimentally. Comparison of experimental and computational data, with the same methods and basis set as those used for the present work, is more than satisfactory. Isotropic hyperfine constants for ^{25}Mg nucleus is well reproduced, −114.4G vs −108.7 G for ^{25}Mg, whereas that for ^{1}H is somewhat overestimated by calculations, 7.9 G vs 4.2 G. Calculated and experimental dipolar terms coincide. Also for the MgH radical, the agreement between experimental and computed values is remarkable. In this case, the isotropic coupling constant for the ^{25}Mg atom is slightly underestimated, −67.8 G vs −78.5 G, whereas that of ^{1}H atom is again overestimated, −131.7 G vs 105.6 G. The dipolar terms are almost exactly reproduced. Therefore, we conclude that the methodology applied in this work to compute EPR quantities of electrons trapped at Mg cationic sites of MgO surface, in the vicinity of an adsorbed proton, is robust enough to produce reliable data for ^{25}Mg nuclei. However, hyperfine constants computed for protons might be slightly overestimated.

Moreover, it must be commented that trapped electrons in insulators are not always properly described at the DFT level since this approach tends to exaggerate the delocalized nature of unpaired electrons.[37] Hybrid functionals have shown to provide more accurate answers in several cases. However, the importance of these aspects should be considered when comparing theory to experiment.

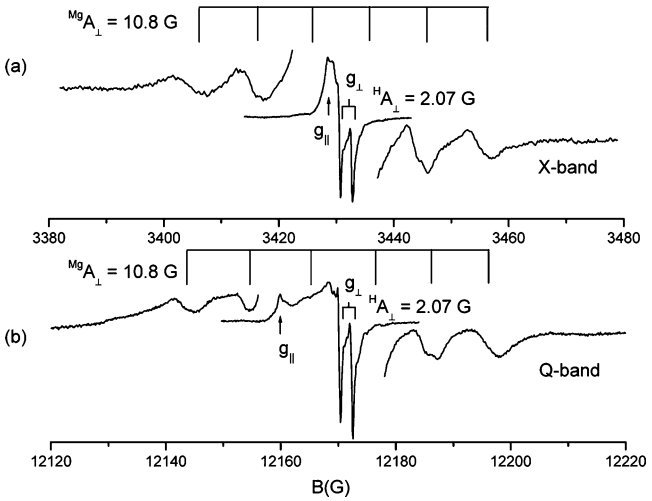

Figure 2. EPR spectrum of excess electron centers generated at the surface of unquenched MgO. (a) X-band frequency and (b) Q-band frequency. The stick diagrams evidence the ^{25}Mg hyperfine splitting relative to species A.

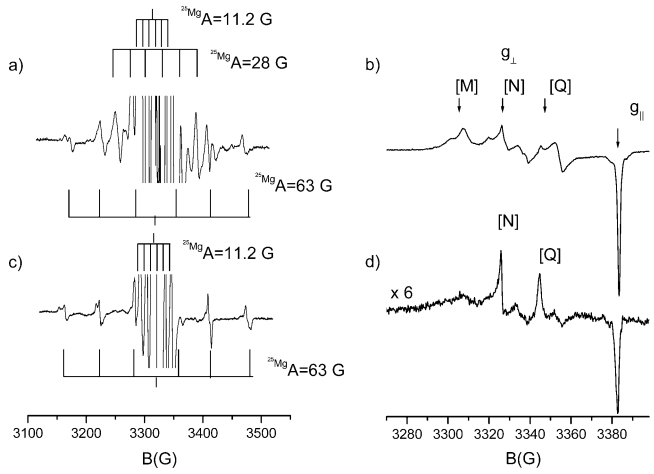

Figure 3. EPR spectra recorded at X-band frequency of; (a) excess electron centers generated on quenched MgO powders, (b) O^- ions generated by reaction of N_2O with surface excess electrons (spectrum a), (c) excess electrons generated in the dark by reaction of H_2 with surface O^- ions (see text), (d) O^- ions generated by reaction of N_2O with surface excess electrons generated in the dark (spectrum b).

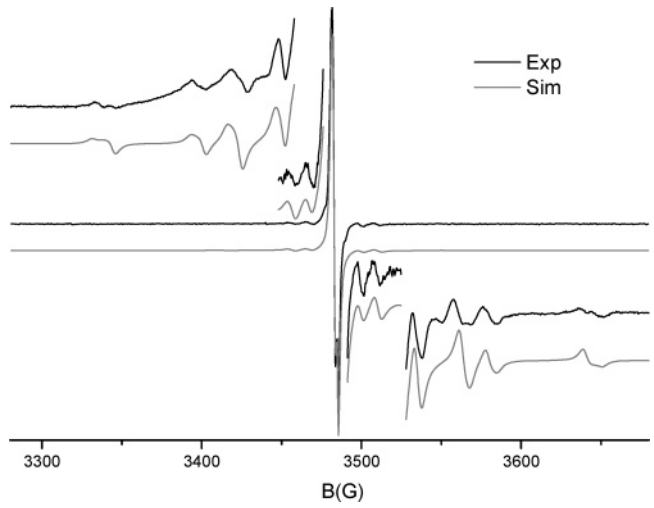

Figure 4. Experimental and simulated EPR spectrum of surface excess electrons generated on the quenched MgO sample.

4. Results and Discussion

4.1. EPR Spectra of Electron Centers after Irradiation of Rapidly Quenched Mg. Surface trapped electrons, generated on thermally activated, unquenched MgO, exhibit the EPR spectra reported in Figure 2 at 9.5 (X band, Figure 2a) and 35 GHz (Q-band, Figure 2b), respectively.The Q-band spectrum nicely confirms the assignments made in the past from the analysis of the X band spectrum.[25] The signal is dominated by an axial feature split in two lines, in correspondence of the perpendicular direction, by the interaction with the H nucleus (nuclear spin $I = 1/2$) belonging to the OH group located nearby the trapped electron. A second hyperfine structure is due to ^{25}Mg (nuclear spin $I = 5/2$, natural abundance 10%) and appears as a weak sextet (the coupling constant is 11 G) in the spectrum. The small abundance of the ^{25}Mg isotope is the reason why, whatever the number of Mg ions surrounding the trapped electron, the trace of only one of them appears in the spectrum (the hyperfine sextet). This dominating species ($g_\perp = 1.9996$, $g_\parallel = 2.0014$, $A_\perp$(H) = 2.07G, $A_\perp$(Mg) = 10.8G, $A_\parallel$(Mg) = 11.2) will be hereafter labeled as species [A]. It should be noted that even though the A tensor measured from the EPR spectrum appears to be axial, ^{1}H ENDOR measurements performed in the past[38] revealed a nonaxial ^{1}H *A* tensor with $A_1 = 2.07$ G, $A_2 = 2.00$ G, and $A_3 = 0.31$ G. The presence of such a tiny anisotropy which remains undetected in CW-EPR even at Q-band frequencies is however important in that indicates that the local symmetry of the trapped electron site is lower than axial. The multifrequency approach combined with computer simulation of the spectrum allows us to reliably identify the spin Hamiltonian parameters of the dominant species but also confirms that more than one type of centers contributes to the whole spectrum. This is also evidenced by results from the decomposition of nitrous oxide on the system (N_2O reacts with the unpaired electron producing surface stabilized O^- ions) which produces a series of distinct O^- species clearly reflecting the heterogeneity of the surface centers, not fully appreciable by the EPR spectra of the original electron traps.[39] These latter spectra (Figure 2) are not sufficiently resolved to allow a clear and detailed assignment. In other words, the most evident spectral features (g values and ^{1}H hyperfine constant, Figure 2) are not sensitive enough to allow discrimination among various trapped electron species. This limitation has been recently superseded when two new ^{25}Mg hyperfine sextets have been identified.[23] To increase the intensity of the spectrum so to gain extra resolution we quenched the sample at the end of thermal activation bringing the powder from 1173 to 77 K as described in the Experimental Section. In this case more intense spectra are obtained which are qualitatively equal to those shown in Figure 2 but which have a better defined ^{25}Mg hyperfine structure. Figure 3a reports the over-amplified spectrum of the rapidly quenched material after UV irradiation in hydrogen. Three distinct ^{25}Mg hyperfine structures are observed, the first one (out of scale in the present figure) being the same visible in Figure 2a and related to species [A]. The two other structures are also sextets centered at (or very close to) the same *g* values of the previous one and their features obtained by spectral simulation (vide infra) are $A_\perp$(Mg) = 27G, $A_\parallel$(Mg) = 28G for the more intense sextet (corresponding to a species hereafter labeled as species [B]) and $A_\perp$(Mg) = 59G, $A_\parallel$(Mg) = 63G for the weaker one (species [C]). The latter sextet is the same previously observed in an experiment performed by laser irradiation of the sample in the presence of hydrogen.[23] The relative abundance of the three species has been evaluated by spectral simulation (Figure 4) which shows that species [A] represent about 80% of the species having a visible Mg hyperfine, whereas [B] and [C] represent about 10% and 8% respectively. A deeper insight in the ^{25}Mg hyperfine

TABLE 1: Experimental and Computed g-tensors and Hyperfine Coupling Constants for the Various Trapping Centers on MgO Surface

					^{1}H			^{25}Mg			^{17}O[a]		
	Ab %	g_z	g_x	g_y	A_z	A_x	A_y	A_z	A_x	A_y	A_z	A_x	A_y
[A] exp	80	2.0014	1.9996		0.5	2.07		11.2	10.8		51.0	49.8	
					0.31[b]	2.00[b]	2.07 [b]						
											9.8	9.2	
step, theory		2.00134	1.99943	2.00030	1.2	−8.0	−5.7	−16.9	−15.4	−15.4	−61.1	−54.1	−55.5
											−7.4	−5.3	−5.3
edge, theory		2.00197	1.99949	2.00027	1.1	−8.5	−6.1	−15.7	−14.3	−14.3	−58.6	−55.6	−56.7
											−8.4	−6.9	−6.9
[B] exp	10	2.001	1.999		unres	unres		28	27		unres	unres	
reverse corner, theory		2.00133	2.00030	2.00040	2.5	−7.4	−5.6	−35.5	−31.7	−31.8	−32.2	−26.5	−26.7
[C] exp	8	2.001	1.999		unres	unres		63	59		unres	unres	
corner, theory		2.00204	1.99953	2.00087	1.4	−4.5	−2.9	−64.0	−59.6	−59.7	−15.0	−10.4	−10.4
kink, theory		2.00168	1.99964	2.00060	0.1	−5.1	−2.4	−64.6	−61.1	−61.1	−17.8	−13.2	−13.4
$F_s(H)^+$, theory		2.00085	2.00024	2.00060	1.1	−3.8	−2.1	−8.8	−7.3	−7.3	−33.8	−27.8	−27.8

[a] For [A] site, the two entries for nonequivalent ^{17}O atoms are assigned to (1) ^{17}O in OH group and (2) neighboring ^{17}O lattice ions. [b] Data taken from ref 38.

structures reveals that, as expected, all lines are split in two by the weak interaction with the proton of the OH group. The whole result of the spectral simulation is reported in Table 1. Reexamining spectra obtained by the classic procedure, it becomes clear that the use of rapid quenching of the activated solid does not lead to new species but rather to an enhancement of the number of surface electron trapping sites.

Additional information on the structure of the electron trapping sites can be derived by analysis of the spectra recorded in the case of ^{17}O containing magnesium oxide (Mg^{17}O). The solid was prepared by a particular method described elsewhere[40] and contains a remarkable amount of isotopically labeled O_2^- ions in the most reactive locations of the surface. The ^{17}O spectrum recorded for trapped electrons on this oxide, and generated by the same procedure described before, is reported in Figure 5 and exhibits a symmetric line characterized by the hyperfine structure due to two magnetically nonequivalent ^{17}O nuclei, the first having $A(^{17}O) = 51$G and the second $A(^{17}O) = 9$G. Due to the high degree of local ^{17}O enrichment this intense structure overwhelms all the ^{25}Mg sextets. The ^{17}O structure observed must be due to the most abundant species [A] (80%), whose hyperfine constants (and spin densities) for all the surrounding atoms (H, Mg, O) are now available thanks to the recent, previously mentioned, advances.[40] The described spectrum

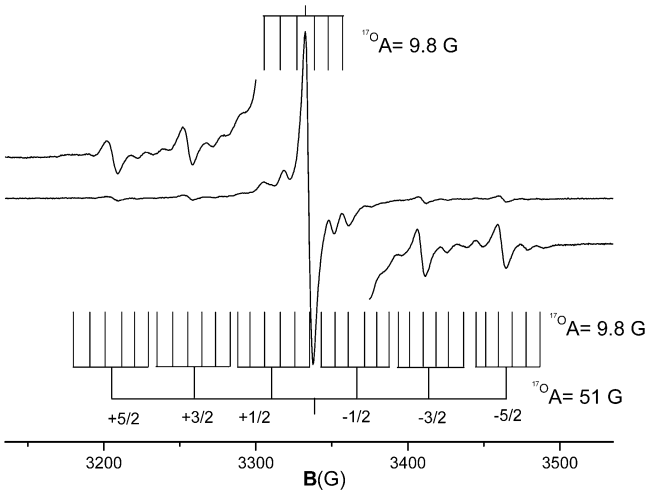

Figure 5. EPR spectrum of surface excess electrons generated on ^{17}O enriched MgO. The stick diagrams refer to the hyperfine splitting patterns relative to two nonequivalent ^{17}O nuclei.

basically indicates that part of trapped electron spin density is inhomogeneously shared by two kinds of oxygens: one is the oxygen of the hydroxyl group which is known to polarize the electron density[41] and the others are neighboring surface oxygens.

4.2. Bleaching by N_2O of the Colored Surface: O^- Formation and Second Generation of Electron Centers. It is well-known that the MgO surface containing trapped electron centers is extremely active in electron-transfer reactions toward various adsorbed species. The particular case of reactivity with nitrous oxide, leading to gaseous nitrogen and surface adsorbed O^- species (2), has been thoroughly investigated in the past[42]

$$Mg_n^{2+}(e^-) + N_2O \rightarrow Mg_n^{2+}(O^-) + N_2 \qquad (2)$$

When the sample, whose spectrum is reported in Figure 3a, is contacted with nitrous oxide one obtains the spectrum of Figure 3b. This spectrum, whose intensity is close to that of Figure 3a, is due to several O^- species, simultaneously present at the surface, with the same $g_{\parallel}$ and different $g_{\perp}$. The main species present in the spectrum, labeled according to the nomenclature proposed by Knözinger and co-workers[15] as species [M], [N], and [Q] are not in the same quantitative ratio of the [A], [B], and [C] species revealed by EPR of the electron centers: this does not allow to establish a direct correspondence between an electron center and a given O^- species and suggests a complexity of the bleaching reaction likely due to some mobility of the O^- species after formation and before stabilization at the surface. However some interesting insights concerning the problem of the correspondence between the various trapped electron centers and the surface O^- ions observed upon reaction with N_2O can be obtained by the reaction of the latter ones with molecular hydrogen. In fact, after N_2O bleaching and O^- formation, the sample reacts with H_2 in the dark giving rise to a second generation of trapped electron centers (reactions 3 and 4, Figure 3c) which can be, in turn, bleached by N_2O (Figure 3d)

$$Mg_n^{2+}(O^-) + H_2 \rightarrow Mg_n^{2+}(H) + H^{\bullet} \qquad (3)$$

$$H^{\bullet} + Mg_n^{2+} + O^- \rightarrow Mg_n^{2+}(e^-)(H)(O^-) \qquad (4)$$

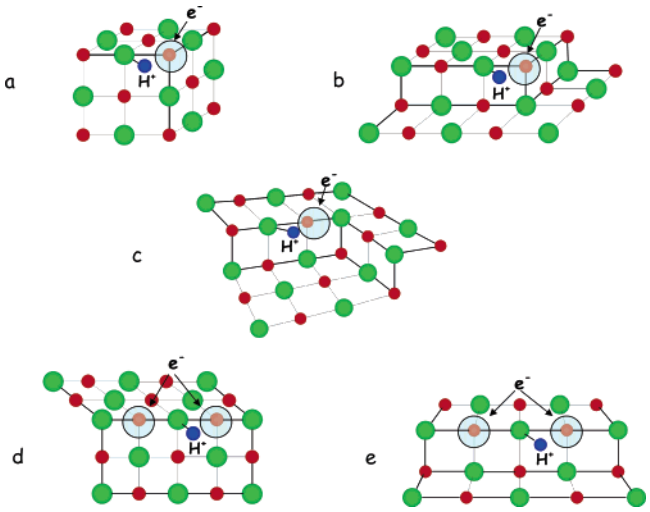

Figure 6. Schematic representation of $(H^+)(e^-)$ pairs formed at various sites of the MgO surface and accounting for the paramagnetic centers of type [A], [B], and [C]. Species [C] corresponds to $(H^+)(e^-)$ pairs formed at Mg_{3c} ions at corners (a) or kinks (b); species [B] corresponds to $(H^+)(e^-)$ pairs formed at Mg_{4c} ions in correspondence of a reverse corner (c); species [A] corresponds to $(H^+)(e^-)$ pairs formed at Mg_{4c} ions formed at edges (d) or steps (e).

The spectra of the second generation are about five times less intense than those of the first generation. When parts a and c of Figure 3 are compared, it can be easily deduced that the quantitative ratio among the various trapped electron species changes going from the first to the second generation, the main reason being the absence of species [B] (30 G coupling constant) in the new spectrum (Table 1). This species lacks because all of the corresponding sites have reacted during the first cycle of activation and bleaching of the solid. This observation is paralleled by another one indicating that in the second generation of O^- ions (Figure 3d) the [M] species is also practically absent. This allows us to establish a reasonable correspondence between species [B] of the electron centers and species [M] of the O^- anions and to suggest that the latter one arises from bleaching of the electron centers of type [B].

4.3. Assignment for the Trapping Electron Centers. Three distinct electron trapping sites, [A], [B], and [C], have been detected on the basis of the ^{25}Mg hyperfine coupling constants. Site [C] is the less abundant (8%) and is characterized by the highest hyperfine constant ($a_{iso} = (2A_\perp + A_{||})/3 = 60.3$ G). This value, if compared with the calculated A_0 value for ^{25}Mg (the expected a_{iso} for a single electron in Mg 3s orbital) which is about 173G, indicates that the trapped electron interacts with one single surface Mg^{2+} ion. This latter ion must produce a very large electrostatic potential to stabilize an electron with the only assistance of a nearby proton, H^+, bound to an oxide anion. Site [C] was also reported after laser irradiation of MgO in the presence of hydrogen.[23] Theoretical modeling indicated that the electron is stabilized by a single Mg_{3c} ion associated to a nearby proton, H^+, bound to an oxide anion (Figure 6, parts a and b). No other location at the surface can reproduce such a large ^{25}Mg hyperfine constant (computed $A_z = -64.0$G and $A_y \sim A_x = -59.7$G for corner and $A_z = -64.6$G and $A_y \sim A_x = -61.1$ for kink vs experimental $|A_z| = 63$G and $|A_y| = |A_x| = 59$G, Table 1). Three-coordinated ions are present at the surface of MgO at corners and kinks of the microcubelets constituting the powder. Since among all of the differently coordinated ions present at the surface (basically 5c, 4c, and 3c) the three-coordinated ones are less abundant, this interpretation also agrees with the low concentration of [C] center.

The site labeled with [B] has also low abundance but lower coupling constant ($a_{iso} = 27.3$G) then site [C]. When bleached by N_2O it origins the O^- species [M] having $g_\perp = 2.042$. Theoretical modeling suggests that ^{25}Mg coupling constant of site [B] is compatible with a number of potential electron trapping sites: in particular models based on electrons trapped in low-coordinated oxygen vacancies (like those in Figure 1, parts b and c) nearby a proton, H^+, bound to an oxide anion, give calculated constants not very far from that observed in this case. However, there are convincing reasons which suggest to assign species [B] to a reverse corner (RC) site (Figure 6c):

(a) The ^{25}Mg calculated hyperfine constants for an electron in a RC site is the closest to the observed values (computed $A_z = -35.5$G and $A_y \sim A_x = -31.8$G vs experimental $|A_z| = 28$G and $|A_y| = |A_x| = 27$G, Table 1);

(b) The surface site originating [B] (trapped electron) and [M] (O^-) centers is, as defined in ref 42, a hot site i.e., it is capable of splitting the hydrogen molecule. Theoretical investigations on the bare RC site have shown that it is capable of such splitting[16] with all the features (activation energy, energy released, stretching frequencies of the adsorbates) observed in the experiments;

(c) The site is a neutral morphological defect certainly present at the surface of activated MgO powders (vide infra) while the vacancies (F_S^{2+} charged defects) present high energy cost and consequently much lower abundance.

It is thus reasonable to assign species [B] to electrons trapped at the reverse corner site (Figure 6c). The fact that the corner, the kink and the reverse corner sites (which are in structural terms complementary) are present in very similar abundance corroborates the above assignment. Notice that the ^{17}O coupling constants that have been computed for sites [B] and [C], Table 1, cannot be directly compared to the experiment since this feature could not be resolved in the spectra due to the relatively low abundance of sites [B] and [C].

Site [A] is the most abundant at the surface and is characterized by the lowest coupling between the electron and ^{25}Mg nuclei. Additional information derived from experiments with $Mg^{17}O$ (Figure 5, Table 1) suggests the presence of two O atoms in symmetric position with respect to the trapped electron, one of which is bound to the proton, H^+. Such a linear display of atoms is compatible with two locations at the surface, i.e., the edge of a cubic crystal and the step, both are one-dimensional morphological line defects (Figure 6, parts d and e). The step and edge sites (which are rather abundant on finely divided MgO powders), among all those simulated by theoretical calculations, exhibit a set of hyperfine constants close to the experimental values for site [A]. In particular both ^{25}Mg ($A_z = -16.9$G and $A_y = A_x = -15.4$G for step and $A_z = -15.7$G and $A_y = A_x = -14.3$G for edge vs an experimental value of $|A_z| = 11.2$G and $|A_y| = |A_x| = 10.8$G) and ^{17}O ($A_z = -61.1, -7.4$G, $A_y = -55.5, -5.3$ and $A_x = -54.1, -5.3$G for step and $A_z = -58.6, -8.4$G, $A_y = -56.7, -6.9$G and $A_x = -55.6, -6.9$G for edge vs the experimental $|A_z| = 51.0, 9.8$G and $|A_y| = |A_x| = 49.8, 9.2$G) computed values acceptably reproduce the experimental ones. The experimentally observed magnetically nonequivalence between the oxygen belonging to the OH group and the other lattice O^{2-} ions is fairly reproduced by the present calculations. The substantial convergence of the two type of constants (^{25}-Mg and ^{17}O) is not observed for any other site and in particular it is not observed for the vacancy at the (100) crystal face. Site [A] can thus be confidently assigned to $(e^-)(H^+)$ pairs at step and edge sites of the MgO surface. It should be noted that for these two sites only the symmetric configuration of the proton

H^+ has been considered (see Figure 6, parts d and e) since it has been shown in a previous paper[16] that the proton flips so fast between the two tilted configurations that the lattice ions cannot follow its motion but fluctuate near their positions. The result is that the proton moves in a single rather than in a double well potential, which is well represented by the symmetric configuration.

Experimental hyperfine coupling constants with ^1H nucleus are also available for site [A], as reported in Table 1. In general, they are very small, indicating that only the tails of the unpaired electron wave function apparently interacts with the hydrogen nucleus. The computed values are considerably larger than the experimental ones, in particular for the dipolar component. Overestimation of the dipolar matrix elements has not been observed in the case of MgOH and MgH, as discussed in the section of Computational Details. One reason could be that the delocalized nature of the trapped electron is overestimated by the DFT approach, despite the use of a hybrid exchange functional. We performed two checks in order to improve our understanding of this problem. First, we evaluated the hyperfine coupling constants for the step site using the Hartree−Fock exchange in combination with the LYP[27] correlation functional (HF/LYP). The increase of HF contribution to the exchange functional should reduce the spurious DFT delocalization. This effect is actually observed on the isotropic coupling constant (−2.3 G) which is considerably reduced with respect to B3LYP (−4.3 G) but is still larger than the experimental value (−1.3 G). On the other hand, the dipolar matrix is almost unaffected by the exchange functional. Second, we checked if, for the case of molecular radicals such as $OH^\bullet$ and $OOH^\bullet$, where the unpaired electron is rather localized, the experimental values are well reproduced. In the case of OH radical in the MgO_2 matrix,[43] the experimental data are the following: $a_{iso} = -27.36$G and the dipolar B matrix result from the sum of $(2b\ -b\ -b)$ and $(b'\ -2b'\ b')$, with $b = -8.51$G and $b' = 19.02$G. The computed values, using the same method and basis set of the present work, are $a_{iso} = -23.62$G, $b = -13.2$G, and $b' = 18.9$G. As far as OOH is concerned, the following experimental values are reported in the literature:[44] $|A_1| = 13.99$G, $|A_2| = 3.57$G, and $|A_3| = 15.67$G, where A_i are the diagonal components of the hyperfine matrix A, comprehensive of both isotropic and dipolar components. We compute $A_1 = -14.27$G, $A_2 = 3.21$G, and $A_3 = -16.75$G. The agreement is substantial in both the examples considered. We can only register some overestimation for the dipolar part relative to the OH radical. Thus the conclusion we draw is that the particular delocalized nature of the trapped electron on the MgO surface may not be described with complete accuracy in all of the details by current methods. Larger errors may thus be observed for very small hyperfine coupling constants, as it is the case for ^1H.

Another reason of the overestimation of the H hyperfine coupling parameters may be envisaged considering the possibility that nanocrystal edges and steps become decorated with excess electrons. The effects related to the formation of small linear chains of mutually interacting centers have not be considered at the present stage of the computational work and may explain the relatively small discrepancy between experiment and calculations. This topic is currently under investigation in our laboratories.

In Table 1 also experimental and computed g-matrix values are reported. The agreement is remarkable since in all cases it is possible to observe a relatively small negative shift from the free electron g value ($g_e = 2.0023193$) for the z component, whereas a larger deviation of the same sign for the x and y components. Since g_x and g_y components are very similar, the system presents almost uniaxial symmetry, which explains the impossibility to resolve the experimental signal completely.

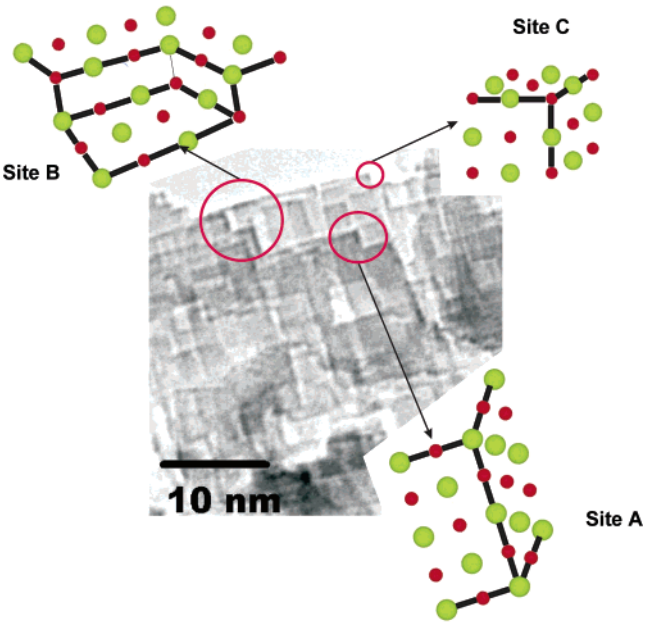

Figure 7. HRTEM microscopy of high surface area MgO powder. The electron trapping sites discussed in the text are highlighted and represented in terms of the corresponding atomistic models.

The three main species observed on the EPR spectrum of surface trapped electron on MgO are thus assigned to distinct sites having in common the fact that they all belong to a family of neutral features connected to the morphology of the body of very tiny microcrystal that compose the solid. All of the three sites are capable, as forecast by density functional calculations reported in the present paper, to react with atomic hydrogen causing its ionization with formation of a surface stabilized electron−proton pair. The same does not apply for other sites available at the surface (vide infra). This interpretation does not involve the presence of charged oxygen vacancies (F_S^{2+}) in high concentration and thus overcomes the open problems connected to previous assignments, namely the high energetic cost of the anion vacancy formation and the need to assume the presence of compensating cationic vacancies to maintain electroneutrality. This interpretation is also supported by the high resolution transmission electron microscopy (HR-TEM) pictures (Figure 7) which reveals microcrystalline MgO as a body of small, regularly interpenetrated, cubic crystals in which the dominating surface is the (100) one. In the figure, it is also possible to identify the presence of crystal corners (site [C]) and of morphological features related to the ordered assembly of the interpenetrated cubic crystals, i.e., reverse corners (site [B]), edges (site [A]), and reverse edges. The sites discussed above can be easily identified on the micrograph and correspond to the atomistic models originating from the coupled spectroscopic and theoretical investigation. It must be noted that localized electron trapping is observed only in the presence of low-coordinated cations. In fact we found, for example, that the reverse edge, originating at the intersection of two perpendicular planar faces, is not a proper trapping site since all of the Mg cations are 5-fold coordinated. Moreover, the electron is highly attracted by the proton. The position of the proton on the surface determines the cationic sites where the electron is trapped.

5. Conclusions

For many years, it has been assumed that the paramagnetic centers generated by chemical treatment of ionic oxides (doping by alkali metal or hydrogen) consist of oxygen vacancies filled by one electron. The model is that of an empty oxygen vacancy precursor, the F_S^{2+} center, which binds an electron donated from the adsorbed alkali metal or hydrogen atom forming a F_S^{+} color center. The resulting alkali metal cation or proton are stabilized at a nearby surface oxide anion. This model accounts for a number of observations but is not consistent with the high number of F_S^{2+} precursors that should exist on the surface to explain the amount of paramagnetic centers generated in the doping process. F_S^{2+} centers in fact have a high formation energy and, being charged, also require an equal number of negatively charged defects (e.g. cation vacancies) to maintain electroneutrality. It should be noted however that some oxygen vacancies can actually form during the final stages of surface hydroxylation according to an hypothesis proposed in ref 45. and involving the loss of some surface oxygen (as water) with resulting formation of oxygen vacancies. Nevertheless, the vacancies generated in this way should be partially eliminated during the final activation of the solid at a temperature (1170 K) high enough to allow ion mobility and partial recovery of the thermodynamic equilibrium.

With the present work, thanks to the development of new preparation techniques which allow a higher resolution of the electron spin resonance spectra and to accurate quantum chemical calculations, it has been possible to show that the color centers are mainly formed at morphological irregularities of the surface and consist of $(H^+)(e^-)$ electron pairs. At least three different kinds of sites, [A], [B], and [C], with relative abundances of 80%, 10%, and 8%, respectively, have been identified which are capable of splitting atomic hydrogen yielding distinct $(H^+)(e^-)$ centers. In this work, we have compared a wide set of measured and computed hyperfine coupling constants of the unpaired electron with the surrounding. Besides the couplings with ^{25}Mg and ^{1}H nuclei, recently also ^{17}O values have become available thanks to the preparation of ^{17}O-enriched MgO samples. On the theoretical side, not only the hyperfine coupling constants but also the g-factors have become available, thus allowing a complete mapping of the sites and a throughout comparison of experimental and theoretical spectra. On this basis, we propose a general assignment of the paramagnetic centers. $(H^+)(e^-)$ pairs formed at Mg_{4c} ions at steps and edges account for species [A], centers formed at Mg_{4c} ions at reverse corners correspond to species [B], and species [C] originates from $(H^+)(e^-)$ pairs formed at Mg_{3c} ions at corners and kinks. The precursor sites do not belong to the class of oxygen vacancies, but are neutral morphological sites characterized by the presence of low-coordinated Mg ions. High-resolution transmission electron microscopy clearly shows a high number of these sites in the microcrystals of high surface area MgO prepared either via chemical vapor deposition or by thermal decomposition of the corresponding hydroxide. We have also considered the bare oxygen vacancy, F_s^{2+}, as the precursor site for the formation of the $(H^+)(e^-)$ pair. These centers are able to dissociate H_2 and to form $F_s(H)^+$ center.[46] The computed g-tensor and hyperfine matrix with the same approach adopted for the other centers are reported at the bottom of Table 1. Although the hyperfine coupling constants for the ^{25}Mg and ^{1}H atoms are in reasonable agreement with the experimental values registered for site [A], those for the ^{17}O atoms are far too small with respect to the experimental data. Therefore, not only the expected abundance of F_s^{2+} precursor sites is too low to explain the number of observed paramagnetic centers, but also the properties of the $F_s(H)^+$ center do not account for the experimental data.

The fact that the paramagnetic centers formed by chemical doping of polycrystalline MgO consist of $(H^+)(e^-)$ pairs, however, does not totally exclude the presence of oxygen vacancies on the surface.[10] Recent studies on the surface coloring experiments by Na doping clearly show that a small fraction of paramagnetic F_S^{+} centers actually exist.[47] Furthermore, recent EPR measurements performed in UHV conditions on thin MgO films have shown the presence of these centers after the surface has been damaged by electron bombardment.[48] It should also be mentioned that conclusions about the relative abundance of surface defects on the MgO surface should not be disjointed by the analysis of the form and of the preparation history of the material. Recent experimental[49−51] and theoretical studies[14] clearly indicate that F_S centers are present on the surface of MgO thin films prepared by direct oxidation of Mg vapor in O_2 background atmosphere on a metal substrate. Other experiments[52] on MgO single crystals suggest that divacancies (missing pairs of Mg and O ions) may play an important role. Thus, although the characteristics of the various surface defects (morphological sites, vacancies, and divacancies) are obviously the same, the relative concentration can be significantly different, opening potential perspectives for the engineering of surface defects in this class of compounds.

Acknowledgment. This work has been supported by a Cofin project 2003. We thank Martin Sterrer, Erich Knözinger, Alex Shluger, and Peter Sushko for several useful discussions. We gratefully thank Dr. Lucia Bonoldi for the Q-band spectrum and Mr. Raffaele Disa for skilful glass blowing of the EPR cell used in the quenching experiment.

References and Notes

(1) Matsuishi, S.; Toda, Y.; Miyakawa, M.; Hayashi, K.; Kamiya, T.; Hirano, M.; Tanaka, I.; Hosono, H. *Science* **2003**, *301*, 626.
(2) Hayashi, K.; Matsuishi, S.; Kamiya, T.; Hirano, M.; Hosono, H. *Nature* **2002**, *419*, 4621.
(3) Ichimura, A. S.; Dye L.; Camblor, M. A.; Villaescusa L. A, *J. Am. Chem. Soc.* **2002**, *124*, 1170.
(4) Edwards, P. P.; Anderson P. A.; Thomas J. M. *Acc. Chem. Res.* **1996**, *29*, 23.
(5) Moissette, A.; Batonneau, Y.; Bremard, C. *J. Am. Chem. Soc.* **2001**, *123*, 1235.
(6) Moissette, A.; Vezin, H.; Gener, I.; Patarin, J.; Bremard, C. *Angew. Chem. Intern. Ed.* **2002**, *41*, 1241.
(7) Peterka, D. C.; Tagenkamp, K.; Schröder, M.; Ernst, W.; Pfnür, H. *Surf. Sci.* **1999**, *431*, 146.
(8) Wendt, S.; Kim, Y. D.; Goodman, D. W. *Prog. Surf. Sci.* **2003**, *74*, 141.
(9) Schaub, R.; Wahlström, E.; Rønnau, A.; Laesgaard, E.; Stensgaard, I.; Besenbacher, F. *Science* **2003**, *299*, 377.
(10) Pacchioni, G. *ChemPhysChem* **2003**, *4*, 1048.
(11) Pacchioni, G.; Pescarmona, P. P. *Surf. Sci.* **1998**, *412/413*, 657.
(12) Illas, F.; Pacchioni, G. *J. Chem. Phys.* **1998**, *108*, 7835.
(13) Scorza, E.; Birkenheuer, U.; Pisani, C. *J. Chem. Phys.* **1997**, *107*, 9645.
(14) Sousa, C.; Pacchioni, G.; Illas, F. *Surf. Sci.* **1999**, *429*, 217.
(15) Sterrer, M.; Diwald, O.; Knözinger, E. *J. Phys. Chem. B* **2000**, *104*, 3601.
(16) Ricci, D.; Di Valentin, C.; Pacchioni, G.; Sushko, P. V.; Shluger, A. L.; Giamello, E. *J. Am. Chem. Soc.* **2003**, *125*, 738.
(17) Diwald, O.; Berger, T.; Sterrer, M.; Knözinger, E. *Stud. Surf. Sci. Catal.* **2001**, *140*, 237.
(18) Tench, A. J.; Nelson, R. L. *J. Colloid Interface Sci.* **1968**, *26*, 364.
(19) de Boer, J. H. *Rec. Trav. Chim.* **1937**, *56*, 301.
(20) Ojame, L.; Pisani, C. *J. Chem. Phys.* **1998**, *109*, 10984.
(21) Ricci, D.; Pacchioni, G.; Sushko, P. V.; Shluger, A. L. *J. Chem. Phys.* **2002**, *117*, 2844.
(22) Sushko, P. V.; Gavartin, J. L.; Shluger, A. L. *J. Phys. Chem. B* **2002**, *106*, 2269.

(23) Chiesa, M.; Paganini, M. C.; Giamello, E.; Di Valentin, C.; Pacchioni, G. *Angew. Chem., Int. Ed.* **2003**, *42*, 1759.
(24) Knözinger, E.; Jacob, K. H.; Singh, S.; Hofmann, P. *Surf. Sci.* **1993**, *290*, 388.
(25) Giamello, E.; Paganini, M. C.; Murphy, D. M.; Ferrari, A. M.; Pacchioni, G. *J. Phys. Chem. B* **1997**, *101*, 971.
(26) Becke, A. D. *J. Chem. Phys.* **1993**, *98*, 5648.
(27) Lee, C.; Yang, W.; Parr, R. G. *Phys. Rev. B* **1988**, *37*, 785.
(28) Weil, J. A.; Bolton, J. R.; Wertz, J. E. *Electron Paramagnetic Resonance*; John Wiley & Sons: New York, 1994.
(29) Neese, F. *J. Chem. Phys.* **2001**, *115*, 11080.
(30) Shusko, P. V.; Shluger, A. L.; Catlow, C. R. A. *Surf. Sci.* **2000**, *450*, 153.
(31) Stevens, W.; Bach, H.; Krauss, J. *J. Chem. Phys.* **1984**, *81*, 6026.
(32) Frisch, M. J.; Trucks, G. W.; Schlegel, H. B.; Scuseria, G. E.; Robb, M. A.; Cheeseman, J. R.; Zakrzewski, V. G.; Montgomery, J. A., Jr.; Stratmann, R. E.; Burant, J. C.; Dapprich, S.; Millam, J. M.; Daniels, A. D.; Kudin, K. N.; Strain, M. C.; Farkas, O.; Tomasi, J.; Barone, V.; Cossi, M.; Cammi, R.; Mennucci, B.; Pomelli, C.; Adamo, C.; Clifford, S.; Ochterski, J.; Petersson, G. A.; Ayala, P. Y.; Cui, Q.; Morokuma, K.; Malick, D. K.; Rabuck, A. D.; Raghavachari, K.; Foresman, J. B.; Cioslowski, J.; Ortiz, J. V.; Stefanov, B. B.; Liu, G.; Liashenko, A.; Piskorz, P.; Komaromi, I.; Gomperts, R.; Martin, R. L.; Fox, D. J.; Keith, T.; Al-Laham, M. A.; Peng, C. Y.; Nanayakkara, A.; Gonzalez, C.; Challacombe, M.; Gill, P. M. W.; Johnson, B. G.; Chen, W.; Wong, M. W.; Andres, J. L.; Head-Gordon, M.; Replogle, E. S.; Pople, J. A. *Gaussian 98*, revision A.6; Gaussian, Inc.: Pittsburgh, PA, 1998.
(33) Francl, M. M.; Petro, W. J.; Hehre, W. J.; Binkley, J. S.; Gordon, M. S.; De Frees, D. J.; Pople, J. A. *J. Chem. Phys.* **1982**, *77*, 3654.
(34) Hehre, W. J.; Ditchfield, R.; Pople, J. A. *J. Chem. Phys.* **1972**, *56*, 2257.
(35) Barone, V. In *Recent Advances in Density Functional Methods*; Chong, D. P., Ed.; World Scientific: Singapore, 1996; Part I.
(36) Brom, J. M.; Weltner, W., Jr. *J. Chem. Phys.* **1973**, *58*, 5322.
(37) Pacchioni, G.; Frigoli, F.; Ricci, D.; Weil, J. A. *Phys. Rev. B* **2001**, *63*, 054102.
(38) Murphy, D. M.; Yacob, A.; Purnell, I. J.; Farley, R. D.; Rowlands, C. C.; Paganini, M. C.; Giamello, E. *J. Phys. Chem. B* **1999**, *103*, 1944.
(39) Di Valentin, C.; Ricci, D.; Pacchioni, G.; Chiesa, M.; Paganini, M. C. Giamello, E. *Surf. Sci.* **2002**, *521*, 104.
(40) Chiesa, M.; Martino, P.; Giamello, E.; Di Valentin, C.; Del Vitto, A.; Pacchioni, G. *J. Phys. Chem. B* **2004**, *108*, 11529.
(41) Diwald, O.; Knözinger, E.; Martra, G. *J. Chem. Phys.* **1999**, *111*, 6668.
(42) Pinarello, G.; Pisani, C.; D'Ercole, A.; Chiesa, M.; Paganini, M. C.; Giamello, E.; Diwald, O. *Surf. Sci.* **2001**, *494*, 95. Chiesa, M.; Paganini, M. C.; Giamello, E.; Murphy, D. M. *Res. Chem. Intermediat.* **2002**, *28*, 205.
(43) Giamello, E.; Calosso, G.; Fubini, B.; Geobaldo, F. *J. Phys. Chem.* **1993**, *97*, 5735.
(44) Wyard, S. J.; Smith, R. C.; Adrian, F. J. *J. Chem. Phys.* **1968**, *49*, 2780.
(45) Coluccia, S.; Baricco, M.; Marchese, L.; Martra, G.; Zecchina, A. *Spectrochim. Acta*. **1993**, *49A*, 1289.
(46) D'Ercole, A.; Giamello, E.; Pisani, C.; Ojamäe, L. *J. Phys. Chem. B* **1999**, *103*, 3872.
(47) Brazzelli, S.; Di Valentin, C.; Pacchioni, G.; Giamello, E.; Chiesa, M. *J. Phys. Chem. B* **2003**, *107*, 8498.
(48) Sterrer, M.; Freund, H.-J. Personal communication.
(49) Kramer, J.; Tegenkamp, C.; Pfnür, H. *Phys. Rev. B* **2003**, *67*, 235401.
(50) Sanchez, A.; Abbbet, S.; Heiz, U.; Schneider, W.-D.; Häkkinen, H.; Barnett, R. N.; Landman, U. *J. Phys. Chem. A* **1999**, *103*, 6172.
(51) Abbet, S.; Riedo, E. Brune, H.; Heiz, U.; Ferrari, A. M.; Giordano, L.; Pacchioni, G. *J. Am. Chem. Soc.* **2001**, *123*, 6172.
(52) Barth, C.; Henry, C. R. *Phys. Rev. Lett.* **2003**, *91*, 196102.